Electrically Conductive Poly(vinyl alcohol) Hybrid Films Containing Graphene and Layered Double Hydroxide Fabricated via Layer-by-Layer Self-Assembly

Dan Chen,[†] Xiaoyan Wang,[†] Tianxi Liu,*[,†] Xiaodong Wang,[‡] and Jing Li[‡]

Key Laboratory of Molecular Engineering of Polymers of Ministry of Education, Department of Macromolecular Science, and Department of Optical Science and Engineering, Fudan University, Shanghai 200433, P. R. China

ABSTRACT In this work, single-layer layered double hydroxide (LDH) nanosheets were prepared by exfoliation of highly crystalline Co−Al−NO_3 LDH. Graphene oxide (GO) nanosheets were prepared by the exfoliation of natural graphite oxides in water. By utilizing the hydrogen-bonding layer-by-layer self-assembly method, poly(vinyl alcohol) (PVA) hybrid films with highly oriented GO and LDH were fabricated. By a simple and effective in situ reduction process, multilayer nanocomposite films containing monolayer dispersed graphene and LDHs can be obtained. It was found that the π-conjugation network within the graphene nanosheets was gradually recovered during the reduction process and a critical time for the formation of conductive paths for electron transfer was obtained. The relatively complete reduced hybrid film exhibited significantly improved electrical conductivity compared with the unreduced one. These heterogeneous composite films with monolayer dispersed and aligned graphene and LDHs are expected to find potential applications in electrodes and multifunctional nanocomposites.

KEYWORDS: hydrogen-bonding assembly • exfoliated nanosheets • hybrid film • electrically conductive

INTRODUCTION

Novel carbon-based nanostructures such as buckminsterfullerene, carbon nanotube, and diamond have stimulated intense research over the past decades owing to their exceptional properties (1−4). Recently, graphene (G), as a single-atom-thick two-dimensional graphitic carbon material, has attracted intense scientific interest because of its extraordinary properties. It was anticipated that graphenes can be used as supercapacitors, nanoelectronics devices, chemical sensors, and mechanically reinforced composite materials (5−9). To date, G has been primarily prepared by the chemical reduction of graphene oxide (GO) because this is a convenient and cost-effective route, holding the potential of large-scale preparation. However, the strong tendency of the monolayer graphene sheets to agglomerate during the chemical reduction process severely restricts the exploration of further applications (10−12). It is of particular importance to prevent the G sheet from aggregating and producing graphene films of uniform thickness (e.g., monolayer) over a large area because most of its unique properties are associated only with the single layer of two-dimensional hexagonally packed carbon lattice. The preparation of monolayer GO dispersed composite materials and the subsequent in situ reduction is considered as an effective method to fabricate G hybrid materials with molecule-level dispersion and maximum interfacial interaction between the nanofiller and the matrix (13, 14).

Layered double hydroxide (LDH), also known as anionic or hydrotalcite-like clay, is consisted of positively charged brucite-like layers and counteranions as well as water in the interlayers. The layered structure and the anion-exchange properties of LDH make them attractive because of their potential applications in the fields of catalysis, separation, sensors, and polymer nanomaterials (15−18). However, LDH usually stacks together during the fabrication of nanocomposites because of the high charge density of the layers associated with a high content of anions. Sasaki et al. and Duan et al. prepared novel LDH/polyelectrolyte ultrathin films by electrostatic layer-by-layer (LBL) self-assembly, which has demonstrated with exceptional uniformity and versatility (16−18). We also found that LDHs can be assembled with polymers by hydrogen-bonding-based LBL method (23).

Recently, the synthesis of organic−inorganic hybrid materials based on graphene has received much attention, as these materials may show some special physicochemical characteristics compared with their individual counterparts (19−26). We found that GO and LDH can be LBL assembled with poly(vinyl alcohol) (PVA) (one nonionic, water-soluble polymer) based on hydrogen-bonding interaction, which can widen the applications of graphene in the organic−inorganic nanomaterial field. Herein, we describe a convenient strategy for producing high-quality PVA/G and LDH hybrid film

* To whom correspondence should be addressed. Tel: +86-21-55664197. Fax: +86-21-65640293. E-mail: txliu@fudan.edu.cn.

Received for review April 5, 2010 and accepted June 7, 2010

[†] Key Laboratory of Molecular Engineering of Polymers of Ministry of Education, Department of Macromolecular Science, Fudan University.

[‡] Department of Optical Science and Engineering, Fudan University.

DOI: 10.1021/am100307v

by in situ reducing the hydrogen-bonding assembled film. The as-prepared multilayer hybrid films may find potential applications in the electrical and magnetic fields because of the potentially existed magnetic properties of Co−Al−LDH and electrical properties of graphene (16, 22, 27, 28).

EXPERIMENTAL SECTION

Materials. PVA (M_w = 85 000−124 000, 98−99% hydrolyzed) was purchased from Sigma-Aldrich. Natural graphite powder (325 mesh) and 50% glutaraldehyde solution were commercially obtained from Alfa-Aesar and Aladdin reagent, respectively. 37% HCl, 98% H_2SO_4, *N*,*N*-dimethylformamide (DMF), 50% hydrazine, 30% H_2O_2, $KMnO_4$, $CoCl_2 \cdot 6H_2O$, $AlCl_3 \cdot 6H_2O$, NaCl, $NaNO_3$, and urea were supplied by China Medicine Co.. All reactants were analytical purity and used as received.

Synthesis and Exfoliation of Co−Al−NO_3 LDH. Co−Al−NO_3 LDH used in this study was synthesized on the basis of a previous report with modification (16). First, $CoCl_2 \cdot 6H_2O$ (0.5 mmol), $AlCl_3 \cdot 6H_2O$ (0.25 mmol), and urea (1.75 mmol) were dissolved in 50 mL of deionized water and then treated in a Teflon-lined stainless steel hydrothermal cell at 98 °C for 24 h. The resulting well-crystallized Co−Al−CO_3 LDH was treated with a salt-acid mixed solution (NaCl-HCl) to obtain the Co−Al−Cl LDH. The Co−Al−NO_3 LDH was prepared by treating the Cl^- intercalated LDH with a conventional anion-exchange process using $NaNO_3$.

A mixture of the Co−Al−NO_3 LDH (0.1 g) and formamide (100 cm^3) was shaken vigorously at room temperature for 2 days to yield a transparent colloidal suspension. The suspension was centrifuged at 2000 rpm for 5 min to remove the unexfoliated LDH nanoparticles.

Preparation of Graphene Oxide (GO) Nanosheets. A modified Hummers method was utilized to synthesize the oxidized graphite powders (29). Typically, 2.5 g of natural graphite, 2.5 g of $NaNO_3$ and 7.5 g of $KMnO_4$ were slowly added to 50 mL of concentrated H_2SO_4 under vigorous stirring below 5 °C. The mixture was then stirred continuously for 1 h at 35 °C to oxidize the graphite. After that, 100 mL of water was added into the mixture and the temperature was increased to higher than 90 °C, and the suspension was maintained at 95 °C for 15 min. The mixture was then poured into 300 mL of deionized water, after that 20 mL of H_2O_2 was added into the suspension. After cooling to room temperature, the solid products were filtered, subsequently washed with 5% HCl aqueous solution and water, and dried to obtain graphite oxide.

The obtained graphite oxide was dispersed in DI water to yield a yellow-brown suspension (1 mg mL^{-1}). In a typical exfoliation process, the suspension was ultrasonicated for 1 h using an ultrasonication bath cleaner, and then centrifuged at 2000 rpm for 5 min to remove the unexfoliated graphite oxide particles.

Layer-by-Layer Self-Assembly of Multilayer Films. PVA was dissolved in DI water to obtain 1 wt % aqueous solution. Prior to the deposition of the multilayer films, the quartz glass slides were cleaned by treatment in a bath of H_2SO_4/H_2O_2 (3/1 by v/v) for 1 h, and then thoroughly rinsed with deionized water and dried under nitrogen flow. As shown in Scheme 1, the heterogeneous ultrathin films were fabricated by applying a cyclic repetition of the following steps: (a) dipping the substrate into exfoliated LDH suspension for 10 min, then thoroughly rinsing it with DI water and drying under a nitrogen flow; (b) dipping into an aqueous solution of PVA for 10 min, then rinsing with deionized water and drying under nitrogen flow; (c) dipping into an suspension of exfoliated GO for 10 min, followed by water washing and nitrogen drying; (d) dipping into a solution of PVA again for 10 min, followed by water washing and nitrogen drying. A series of deposition operations were repeated *n* times to produce multilayer films of $(LDH/PVA/GO/PVA)_n$.

Scheme 1. Schematic of Layer-by-Layer Assembly Procedure

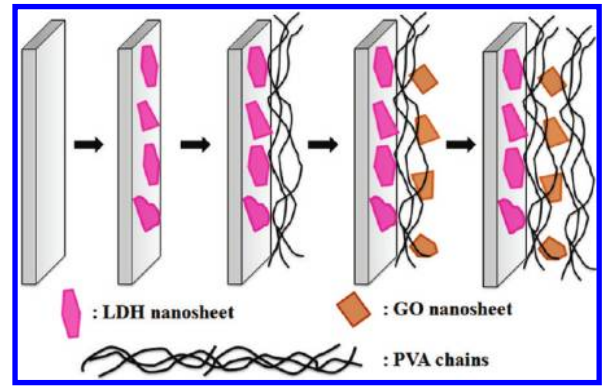

The as-prepared $(LDH/PVA/GO/PVA)_{50}$ hybrid films were cross-linked by immersing into 50% solution of glutaraldehyde for 1 h (30). The thin films containing GO were then reduced by immersing in hydrazine/DMF solution (0.5 mL 50% hydrazine/30 mL DMF) at 85 °C to obtain $(LDH/PVA/G/PVA)_{50}$ films.

Characterization. Scanning electron microscope (SEM, Tescan) performed at an accelerated voltage of 20 kV was used to observe the morphology of the LDH sample, natural graphite and graphite oxide. A field emission scanning electron microscope (SEM, JEOL JSM 6700F) was used to observe the cross-section of the as-prepared multilayer film. X-ray diffraction (XRD) experiments were conducted on a PANalytical (X'Pert PRO) X-ray diffractometer using Cu Kα radiation ($\lambda = 0.154$ nm) at an accelerating voltage of 40 kV and current of 40 mA. UV absorption spectra were obtained on a Lambda 35-vis (Perkin-Elmer) spectrometer. The surface topography and thickness of the exfoliated LDH and GO nanosheets were examined using a NanoScope IV atomic force microscope (AFM) from Digital Instruments. For the characterization of electrical property, all *I*−*V* measurements were made using a Keithley 4200 semiconductor characterization system in ambient atmosphere at room temperature. The measurements were performed under linear sweep mode from −10 to 10 V and the separation between the electrodes was 10 mm.

RESULTS AND DISCUSSION

During the past decades, carbon nanotubes were widely investigated because of their great potential for fabricating high performance materials. Graphene is essentially a carbon nanotube cut along its axis and unrolled to lay flat. Because of their two-dimensional platelike structures, graphene and bilayers containing graphene are zero-gap semiconductors that exhibit larger aerial overlap than carbon nanotubes. Many inorganic layered compounds can be exfoliated into unilamellar nanosheets, which are 2D crystals with thickness on a nanoscale but width on a microscale. By utilizing the exfoliation−reassembly process, polymer chains can be introduced into the reassembled layered compounds to fabricate novel hybrid materials, which are difficult to achieve by conventional methods.

Structure and Morphology of LDH and Its Exfoliated Nanosheets. Figure 1 shows a typical SEM micrograph of Co−Al−CO_3 LDH sample with well-defined hexagonal shape. The urea hydrolysis method and hydrothermal treatment were combined in this study to prepare

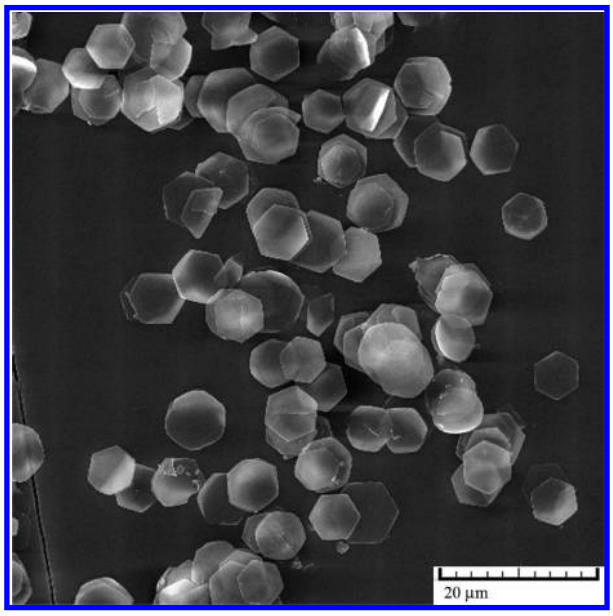

FIGURE 1. SEM micrograph of the as-prepared Co−Al−CO_3 LDH.

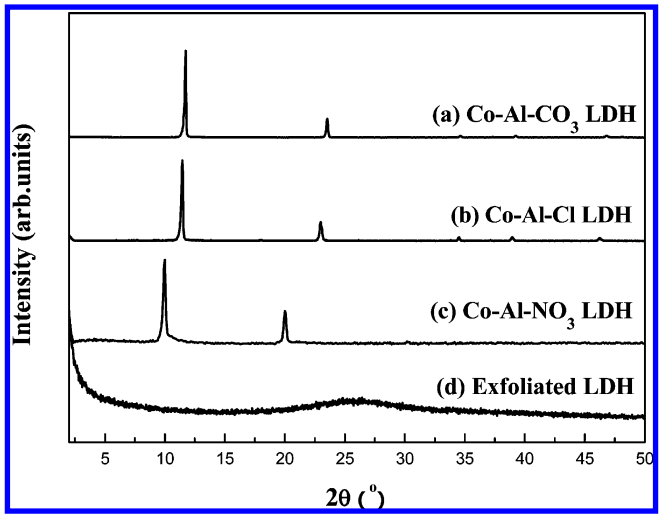

FIGURE 2. XRD patterns of LDH with different intercalated anions as well as the exfoliated LDH powder obtained after centrifugation from LDH colloidal suspension.

the highly crystallized Co−Al−CO_3 LDH. The XRD curve of Co−Al−CO_3 LDH in Figure 2a clearly indicates the high crystallinity of the sample. Co−Al−Cl LDH was employed as the intermediated product because it is difficult to produce fully NO_3^- or bipolar ion intercalated LDH from Co−Al−CO_3 LDH directly. The XRD pattern of Co−Al−Cl LDH in Figure 2b shows that the decarbonation was effective and successful. The basal spacing of LDH was slightly increased from 0.75 nm (for CO_3^{2-} intercalated LDH) to 0.78 nm by the incorporation of Cl^-. As the NO_3^- intercalated LDH was found to possess excellent delamination behavior, Co−Al−NO_3 LDH was synthesized via a conventional anion-exchange process from Co−Al−Cl LDH. As shown in Figure 2c, when being further exchanged by NO_3^-, the interlayer spacing of LDH was increased to 0.89 nm.

By the exfoliation of LDH in formamide, a transparent and pink colloidal suspension can be obtained. The XRD curve of the gel-like aggregate freshly obtained by centrifugating the LDH suspension for 20 min at 30,000 rpm is shown Figure 2d. It can be seen that the obtained unilamellar LDH nanosheets showed only a very broad halo in the 2θ range of 20−30°, arising from the scattering of liquid formamide within the gel-like aggregate of LDH. The absence of the sharp basal reflections of the powdery Co−Al−NO_3 LDH sample indicates the collapse of the ordered layer structure, that is, formation of completely exfoliated structure of LDH. Figure 3a displays the tapping-mode AFM image of LDH nanosheets. Although some fragments of LDH platelets can be seen, nanosheets with lateral dimensions larger than several hundred nanometers can be clearly observed. The height profile (by scanning along the white line marked in Figure 3a) of the nanosheets was shown in Figure 3b. The crystallite terrace of the nanosheets was flat, with an average thickness of about 0.8 nm, which indicated the successful delamination of LDH.

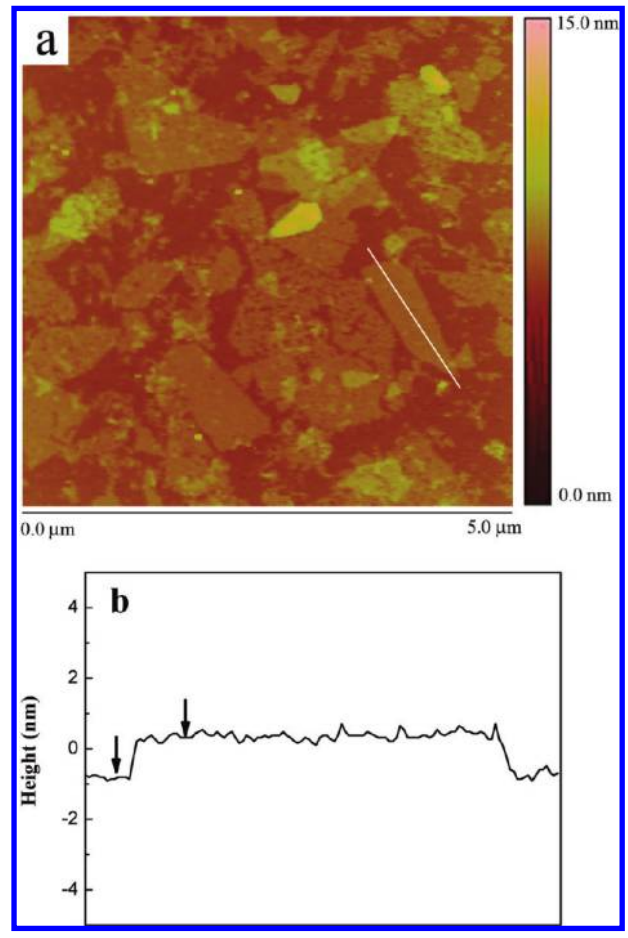

FIGURE 3. Tapping-mode AFM image of the exfoliated LDH nanosheets deposited on a fresh mica substrate.

Fabrication and Characterization of Graphite Oxide and Its Exfoliated GO Nanosheets. To date, graphene can be produced by mechanical cleavage, exfoliation of highly ordered pyrolytic graphite, epitaxial growth, reduction of graphene oxide (GO), etc. Among them, the chemical reduction of GO is considered as the most convenient method. Graphite oxide in this study was synthesized from natural graphite powder by a modified Hummers method. Figures 4 and 5 show the SEM micrographs and

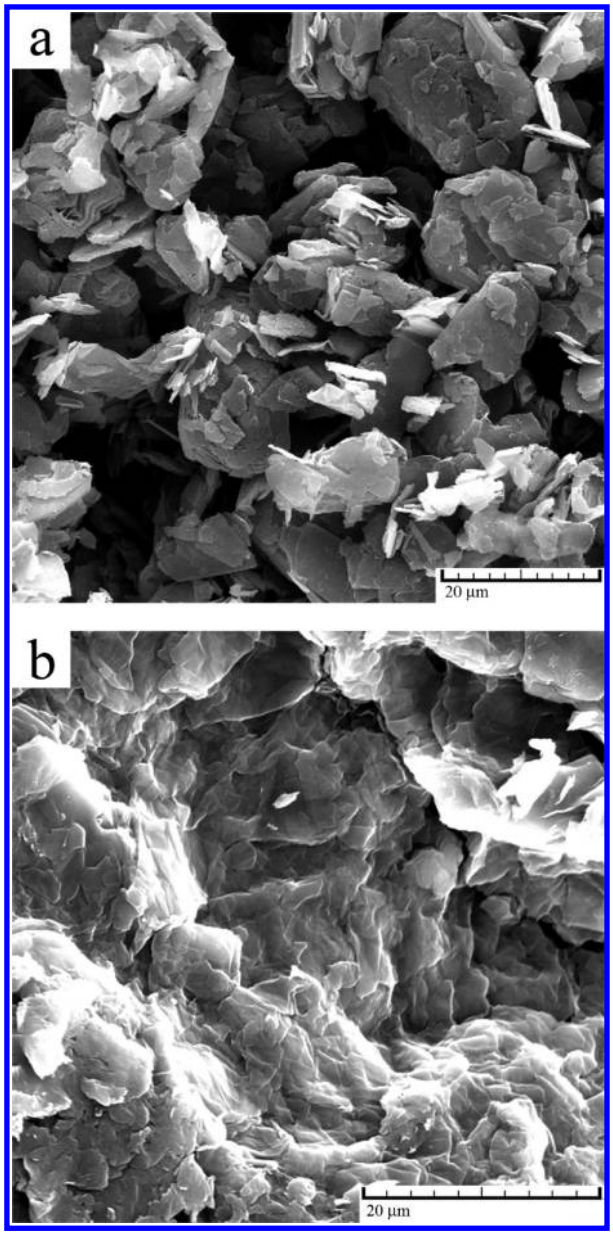

FIGURE 4. SEM micrographs of (a) natural graphite and (b) graphite oxide.

XRD curves of natural graphite and the as-prepared graphite oxide, respectively. It can be seen that the oxidized graphite lost their platelet structure and the crystallinity was comparably decreased after the oxidization. The intense and sharp peak at $2\theta = 26.7°$ of natural graphite shifted to 11.1°, indicating that the interlayer gallery of graphite oxide was expanded from 0.33 to 0.79 nm by the incorporation of various functional groups.

Because of the hydrophilic nature of the oxygenated graphite layers, it is easy to exfoliate in aqueous media. The XRD curve of the gel-like aggregate freshly obtained by centrifugating the GO suspension for 30 min at 30 000 rpm is shown in Figure 5c. It can be seen that the diffraction peak of graphite oxide at $2\theta = 11.1°$ disappeared, indicating complete exfoliation of graphite oxide. The very broad halo in the 2θ range of $20 - 35°$ was attributed to the scattering of water within the gel-like aggregate of GO. In addition, it

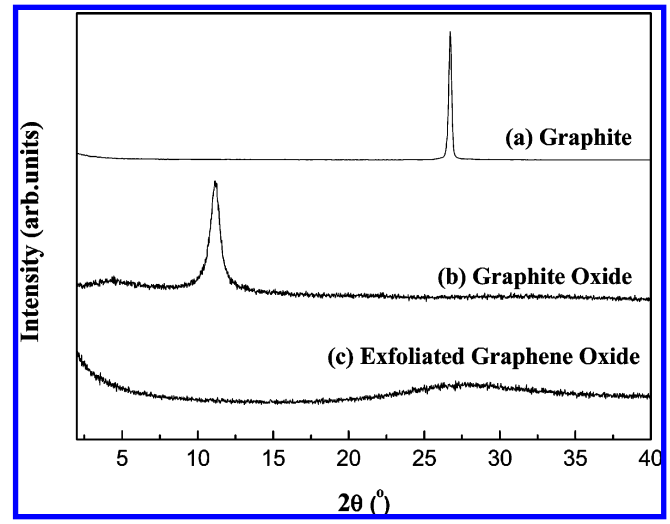

FIGURE 5. XRD patterns of (a) graphite, (b) graphite oxide, and (c) the aggregate obtained by centrifugation from colloidal suspension of exfoliated GO nanosheets.

was interesting to observe that the GO aggregate showed a weak peak at about $2\theta = 7-9°$ (with lower diffraction angle than that at $2\theta = 11.1°$ because of the intercalation of water) when the aggregate was deposited in the air for several minutes. Usually, the exfoliated nanosheets stably exist in their delaminating liquid or media as a colloidal suspension; however, they may reassemble easily when the colloidal system is destroyed. The exfoliated GO restacks much quicker than LDH nanosheets, probably because the GO nanosheets are very soft and can be wrapped up easily by forming aggregates, thus being unable to stably exist without the solvent. The tapping-mode AFM image of the exfoliated GO nanosheets is shown in Figure 6a. As indicated by the height image (Figure 6b), the nanosheets were rather flat and the average thickness was determined to be about 0.8−0.9 nm.

Fabrication and Reduction of LDH/PVA/GO/PVA Multilayer Hybrid Films. As the control of the periodic structures of the hybrid materials over large areas is essential for functional nanomaterial applications, LBL was considered as one of the best methods for fabrication of graphene nanomaterials. The force of hydrogen bonding, which is arguably the strongest van der Waals interaction, was employed as the driving force for LBL assembly in this study (23, 30). PVA, as one kind of uncharged, water-soluble polymer widely used in the materials science, can be LBL self-assembled with GO and LDH because of the hydroxyl, epoxide, and carboxylate groups on the surface of GO and hydroxyl groups on the surface of LDH nanosheets. It has been reported that hybridization of nanoparticles with other functional nanomaterials usually enhances the attributes of each of the components (22, 31, 32). In this contribution, graphene and LDH were combined together to fabricate the hybrid nanomaterials, which are anticipated to possess multifunctional properties.

As shown in Figure 7a, the subsequent growth of multilayer films was monitored by UV−vis spectroscopy after each deposition cycle. Figure 7b shows the dependence of absorbance at 228 nm against the number of deposition

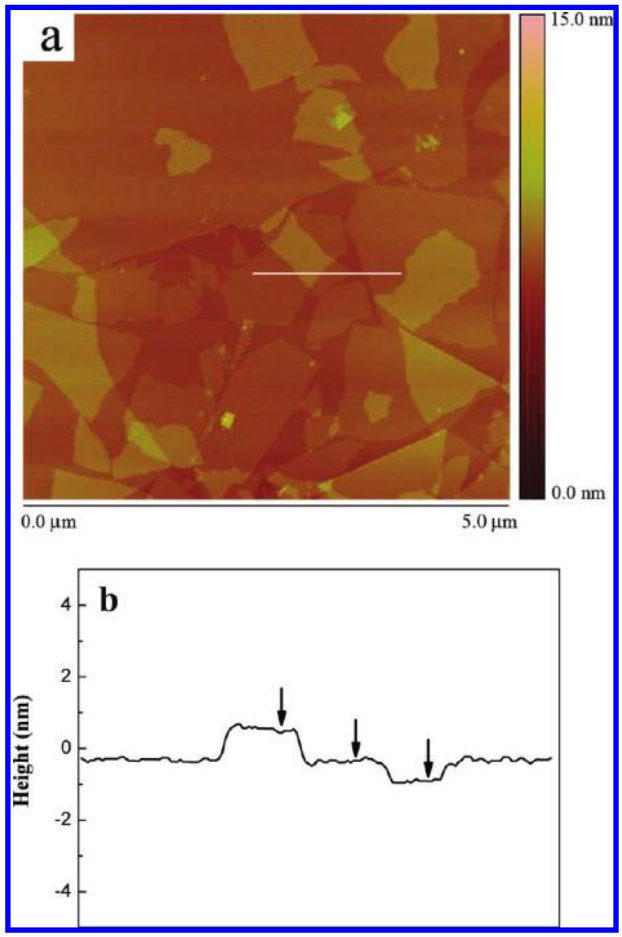

FIGURE 6. Tapping-mode AFM image of the graphene oxide nanosheets deposited on a fresh mica substrate.

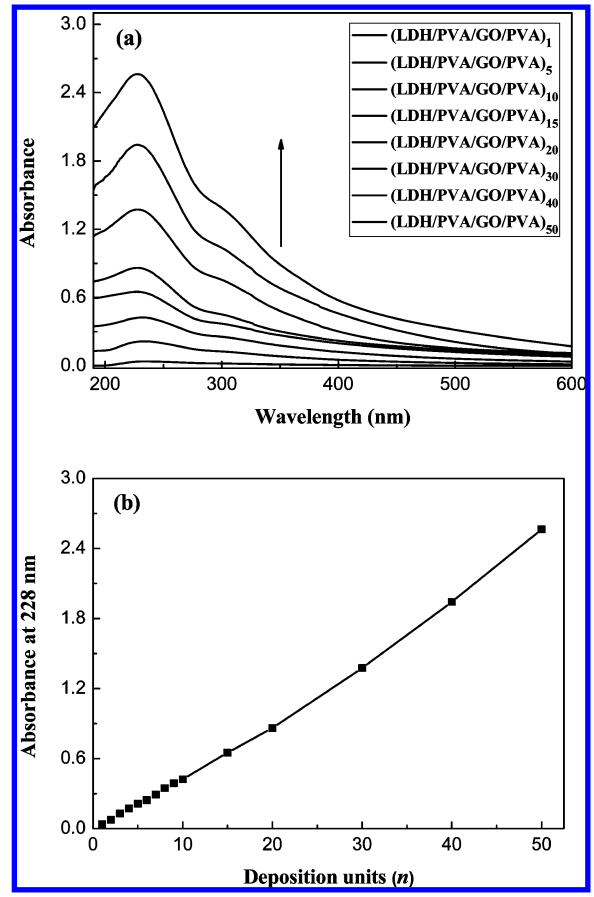

FIGURE 7. (a) UV absorption spectra of the multilayer (LDH/PVA/GO/PVA)$_n$ films; (b) absorbance at 228 nm versus the number of deposition cycles.

units. It can be seen that the absorption increased linearly with the increase in deposition cycles, which indicates a stepwise and regular film growth in thickness.

XRD was also employed to characterize the periodic nanostructure of the multilayer films. As shown in Figure 8, the obtained (LDH/PVA/GO/PVA)$_n$ ultrathin films exhibit a Bragg peak at about $2\theta = 6.4°$, which was attributed to the so-called superlattice reflection of the inorganic/organic periodic nanostructure. It can be seen that the Bragg peak increased as the number of deposition cycle increased. According to the XRD results, the average thickness of one bilayer is calculated to be about 1.4 nm. Therefore, the thickness of multilayer film with 50 units (100 bilayers) is about 140 nm. SEM was employed to observe the side view of (LDH/PVA/GO/PVA)$_{50}$ film. Figure 9 clearly shows a layered structure of the LBL film with a thickness of about 200−300 nm, which was comparably larger than that estimated from the XRD results. That is probably because the LBL assembly is a dynamic process. During the deposition of the multilayers, some weakly bonded polymer chains and nanosheets may be desorbed from the substrate and then reabsorbed to the newly deposited multilayer films. This means that the actual deposition layers may be larger than the real deposition cycles thus leading to a larger film thickness. Besides that, the experimental errors brought about by the XRD and SEM measurements may also lead to the inconsistency in the thickness values.

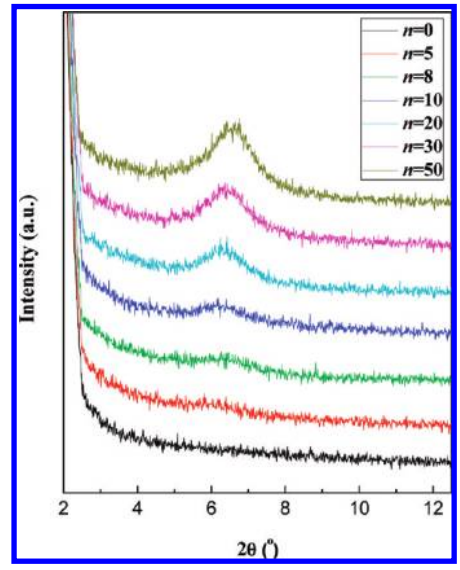

FIGURE 8. XRD patterns of the multilayer assembled films of (LDH/PVA/GO/PVA)$_n$.

As the functional groups bonded on graphene oxide and other atomic-scale lattice defects affect the electrical transport, the reduction of electrically nonconductive GO to highly conductive graphene (G) is necessary. The as-prepared films were reduced by hydrazine to obtain the (LDH/PVA/G/PVA)$_{50}$ multilayer films. As the LBL films are very thin and not as compact as the bulk PVA films, the hydrazine can penetrate

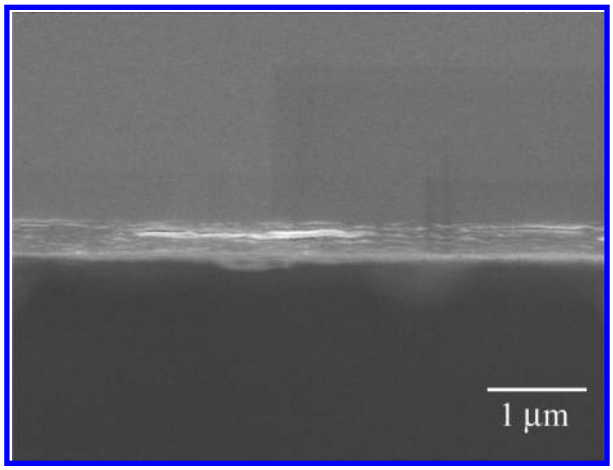

FIGURE 9. Side view of SEM image of the $(LDH/PVA/GO/PVA)_{50}$ ultrathin film.

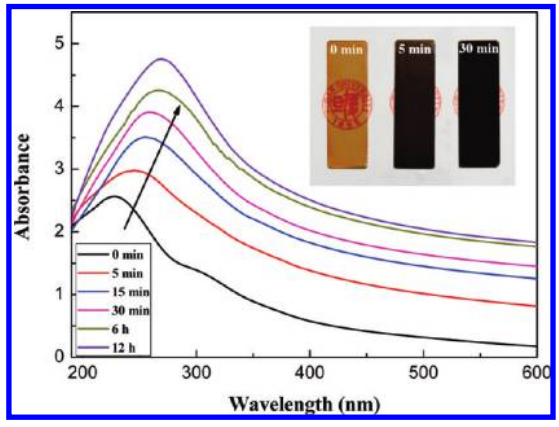

FIGURE 10. UV absorption spectra of the $(LDH/PVA/G/PVA)_{50}$ films that were reduced for different time. The inset graph shows the digital photograph of the unreduced and reduced LBL films.

into the multilayer films thus leading to the relatively complete reduction of GO. Figure 10 shows the UV spectra of the LBL films experienced the reduction treatment by hydrazine for different time (from 5 min, 15 min, 30 min, to 6 to 12 h). The unreduced $(LDH/PVA/GO/PVA)_{50}$ film showed an absorption peak centered at 228 nm and a shoulder at about 300 nm, which could be assigned to $\pi \rightarrow \pi^*$ transitions of aromatic C−C bonds and $n \rightarrow \pi^*$ transitions of C═O bonds, respectively. After the reduction treatment, the absorption of the films in the whole spectral region increased and the main absorption peaks of the films red-shifted gradually from 228 to 272 nm (for 12 h reduction treatment). And, the shoulder absorption peak at higher wavelength became undiscernible gradually. All these observations are indicative of the gradual restoration of the π-conjugation network within the G nanosheets. Moreover, it was found that the red shift of the UV absorption peaks was significant in the early stage of reduction process, and gradually became slow after reducing for more than 30 min. These results were consistent with the macroscopic phenomenon. The inset digital photographs show the films after reduction treatment for 0, 5, and 30 min. It can be seen that the transparent yellow-brown multilayer film was changed into black color significantly after reduction only for 5 min. After reduction treatment for more than 30 min, the films became very dark

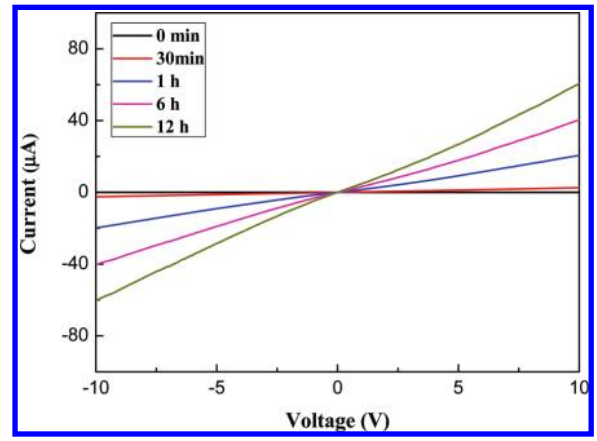

FIGURE 11. Current−voltage plots of the $(LDH/PVA/G/PVA)_{50}$ film samples that were reduced for different time.

and thus the logo printed on the paper under the film cannot be clearly discerned. This was consistent with the significant increase in the absorption in the whole region in the UV spectra.

Figure 11 shows the $I-V$ curves of the $(LDH/PVA/G/PVA)_{50}$ films that were reduced for different time. It was found that both the unreduced and the film reduced for 5 min were insulative and did not show any clear electrical signals. A reduction time of 15 min is the critical time for the formation of conductive paths for electron transfer. Although the UV results indicated that a considerable part of the conjugated network of graphene was recovered after being reduced for 15 min, the electrical current was very low as the presence of a small amount of defects may severely affect the electron transfer. As the current for the 15 min reduced sample was too low to be distinguished from the unreduced film, its $I-V$ curve was not included in Figure 11. After being reduced for more than 30 min, the films became well-conductive, and the electrical conductivity was increased with increasing reduction time. The color change from brown to black discussed above only indicates the partial restoration of the π-conjugation network within the graphene nanosheets. When most of the epoxide groups were restored to C═C upon reduction, the electrons can be smoothly transferred in the whole range of the hybrid films, thus leading to a significant improvement of electrical conductivity. The UV spectra, photographic evidence combined with the electrical measurements, demonstrate the successful fabrication of conductive hybrid films of PVA with graphene and LDH. The as-prepared conductive films can be potentially used in electrode and nanocomposite material fields. By adjusting the film thickness (the deposition units) and the reduction extent of GO, the films can be used as controllable electrode and switches. Moreover, the potential magnetic properties of Co−Al−LDH can also be combined with the electrical properties of the assembled hybrid films, which may find wider applications as the magnetic-electric sensors. The research work in these aspects is still in progress.

CONCLUSIONS

In this contribution, single-layer LDH nanosheets with thickness of 0.8 nm were obtained by delaminating the

anion-exchanged Co−Al−NO_3 LDH. Graphene oxides with thickness of about 0.8−0.9 nm were prepared by the exfoliation of natural graphite oxide powders. By utilizing the hydrogen bonding interaction of both PVA/GO and PVA/LDH, uniform and molecular-level-ordered multilayer hybrid films were fabricated. UV spectroscopy, XRD, and SEM were employed to characterize the as-prepared multilayer films. It was found that the electrical conductivity of the in situ reduced film was significantly improved compared with the unreduced one, and the electrical conductance of the reduced film was improved with increasing reduction time. The heterogeneous films with monolayer dispersed graphene and LDH nanosheets are expected to find potential applications in the magnetic and electrical fields due to their structural diversity and combined functionality. This study possesses a significant advantage for miniaturization of conductive film devices and may open a new way for fabricating ultrathin PVA hybrid films with multifunctionality.

Acknowledgment. This work was supported by the National Natural Science Foundation of China (20774019; 50873027), "Shu Guang" project (09SG02) supported by Shanghai Municipal Education Commission and Shanghai Education Development Foundation, and the Shanghai Leading Academic Discipline Project (Project Number: B113).

REFERENCES AND NOTES

(1) Hasan, T.; Sun, Z. P.; Wang, F. Q.; Bonaccorso, F.; Tan, P. H.; Rozhin, A. G.; Ferrari, A. C. *Adv. Mater.* **2009**, *21*, 3874–3899.
(2) Shang, N. G.; Papakonstantinou, P.; Wang, P.; Zakharov, A.; Palnitkar, U.; Lin, I. N.; Chu, M.; Stamboulis, A. *ACS Nano* **2009**, *3*, 1032–1038.
(3) Wang, C. C.; Guo, Z. X.; Fu, S. K.; Wu, W.; Zhu, D. B. *Prog. Polym. Sci.* **2004**, *29*, 1079–1141.
(4) Vichchulada, P.; Zhang, Q. H.; Duncan, A.; Lay, M. D. *ACS Appl. Mater. Interfaces* **2010**, *2*, 467–473.
(5) Stankovich, S.; Dikin, D. A.; Dommett, G. H. B.; Kohlhaas, K. M.; Zimney, E. J.; Stach, E. A.; Piner, R. D.; Nguyen, S. T.; Ruoff, R. S. *Nature* **2006**, *442*, 282–286.
(6) McBride, J. R.; Lupini, A. R.; Schreuder, M. A.; Smith, N. J.; Pennycook, S. J.; Rosenthal, S. J. *ACS Appl. Mater. Interfaces* **2009**, *1*, 2886–2892.
(7) Wang, S. R.; Tambraparni, M.; Qiu, J. J.; Tipton, J.; Dean, D. *Macromolecules* **2009**, *42*, 5251–5255.
(8) Lui, C. H.; Liu, L.; Mak, K. F.; Flynn, G. W.; Heinz, T. F. *Nature* **2009**, *462*, 339–341.
(9) Kim, S. R.; Parvez, M. K.; Chhowalla, M. *Chem. Phys. Lett.* **2009**, *483*, 124–127.
(10) Zhou, Y.; Bao, Q. L.; Tang, L. A. L.; Zhong, Y. L.; Loh, K. P. *Chem. Mater.* **2009**, *21*, 2950–2956.
(11) Steurer, P.; Wissert, R.; Thomann, R.; Mulhaupt, R. *Macromol. Rapid Commun.* **2009**, *30*, 316–327.
(12) Shen, J. F.; Hu, Y. H.; Li, C.; Qin, C.; Ye, M. X. *Small* **2009**, *5*, 82–85.
(13) Vickery, J. L.; Patil, A. J.; Mann, S. *Adv. Mater.* **2009**, *21*, 2180–2184.
(14) Liang, J. J.; Huang, Y.; Zhang, L.; Wang, Y.; Ma, Y. F.; Guo, T. Y.; Chen, Y. S. *Adv. Funct. Mater.* **2009**, *19*, 2297–2302.
(15) Li, L.; Ma, R. Z.; Ebina, Y.; Iyi, N.; Sasaki, T. *Chem. Mater.* **2005**, *17*, 4386–4391.
(16) Liu, Z. P.; Ma, R. Z.; Osada, M.; Iyi, N.; Ebina, Y.; Takada, K.; Sasaki, T. *J. Am. Chem. Soc.* **2006**, *128*, 4872–4880.
(17) Yan, D. P.; Lu, J.; Wei, M.; Han, J. B.; Ma, J.; Li, F.; Evans, D. G.; Duan, X. *Angew. Chem., Int. Ed.* **2009**, *48*, 3073–3076.
(18) Han, B. J.; Lu, J.; Wei, M.; Wang, Z. L.; Duan, X. *Chem. Commun.* **2008**, *41*, 5188–5190.
(19) Cai, D. Y.; Song, M.; Xu, C. X. *Adv. Mater.* **2008**, *20*, 1706–1709.
(20) Tung, V. C.; Chen, L. M.; Allen, M. J.; Wassei, J. K.; Nelson, K.; Kaner, R. B.; Yang, Y. *Nano Lett.* **2009**, *9*, 1949–1955.
(21) Manga, K. K.; Zhou, Y.; Yan, Y. L.; Loh, K. P. *Adv. Funct. Mater.* **2009**, *19*, 3638–3643.
(22) Pasricha, R.; Gupta, S.; Srivastava, A. K. *Small* **2009**, *5*, 2253–2259.
(23) Huang, S.; Cen, X.; Peng, H. D.; Guo, S. Z.; Wang, W. Z.; Liu, T. X. *J. Phys. Chem. B* **2009**, *113*, 15225–15230.
(24) Kotov, N. A.; Dekany, I.; Fendler, J. H. *Adv. Mater.* **1996**, *8*, 637–641.
(25) Cassagneau, T.; Fendler, J. H. *Adv. Mater.* **1998**, *10*, 877–881.
(26) Wu, J. H.; Tang, Q. W.; Sun, H.; Lin, J. M.; Ao, H. Y.; Huang, M. L.; Huang, Y. F. *Langmuir* **2008**, *24*, 4800–4805.
(27) Kong, B. S.; Yoo, H. W.; Jung, H. T. *Langmuir* **2009**, *25*, 11008–11013.
(28) Wang, D. W.; Li, F.; Zhao, J. P.; Ren, W. C.; Chen, Z. G.; Tan, J.; Wu, Z. S.; Gentle, I.; Lu, G. Q.; Cheng, H. M. *ACS Nano* **2009**, *3*, 1745–1752.
(29) Hummers, W. S.; Offeman, R. E. *J. Am. Chem. Soc.* **1958**, *80*, 1339–1340.
(30) Podsiadlo, P.; Kaushik, A. K.; Arruda, E. M.; Waas, A. M.; Shim, B. S.; Xu, J. D.; Nandivada, H.; Pumplin, B. G.; Lahann, J.; Ramamoorthy, A.; Kotov, N. A. *Science* **2007**, *318*, 80–83.
(31) Kong, B. S.; Geng, J. X.; Jung, H. T. *Chem. Commun.* **2009**, *16*, 2174–2176.
(32) Ramanathan, T.; Abdala, A. A.; Stankovich, S.; Dikin, D. A.; Herrera-Alonso, M.; Piner, R. D.; Adamson, D. H.; Schniepp, H. C.; Chen, X.; Ruoff, R. S.; Nguyen, S. T.; Aksay, I. A.; Prud'homme, R. K.; Brinson, L. C. *Nat. Nanotechnol.* **2008**, *3*, 327–331.

AM100307V